

Ultralow-frequency shear modes of 2-4 layer graphene observed in scroll structures at edgesPing-Heng Tan,^{*} Jiang-Bin Wu, Wen-Peng Han, Wei-Jie Zhao, and Xin Zhang*State Key Laboratory of Superlattices and Microstructures, Institute of Semiconductors, Chinese Academy of Sciences, Beijing 100083, China*

Hui Wang and Yu-Fang Wang

Department of Physics, Nankai University, Tianjin 300071, China

(Received 30 December 2013; revised manuscript received 6 April 2014; published 6 June 2014)

The in-plane shear (C) modes between neighbor layers of 2-4 layer graphenes (2-4LGs) and the corresponding 2-4 layer graphene scrolls (2-4LGSs) rolled up by 2-4LGs at edges are investigated by Raman scattering. In contrast to the result that only one C mode is observed in 3-4LGs, all the C modes of 3-4LGs are observed in 3-4LGSs, whose frequencies agree with the theoretical prediction by the force-constant and linear chain models. The results indicate that the C mode intensity of 2-4LGSs is resonantly enhanced by the electronic transition gaps of band structures of 2-4LGS structures at edges, which makes it possible to observe all the C modes. Indeed, for a simple assumption, the calculated band structures of twisted $(n + n)$ LGs ($n = 2,3,4$) show parallel conduction and valence bands and the corresponding Van Hove singularities in the joint density of states along Γ -M, Γ -K and/or K-M directions. The intensity resonance of the C modes provides direct evidence to explain how the band structure of few layer graphenes can be sensitive to local stacking configurations. This result can be extended to n layer graphene ($n > 4$) for understanding the basic phonon and electronic properties of multilayer graphenes. This observation of all the C modes in graphene scrolls can be foreseen in other two-dimensional materials with similar scroll structures.

DOI: [10.1103/PhysRevB.89.235404](https://doi.org/10.1103/PhysRevB.89.235404)

PACS number(s): 81.05.ue, 63.22.Rc, 73.22.Pr, 78.67.Wj

I. INTRODUCTION

Single-layer graphene (SLG) is of high mobility and optical transparency, as well as high flexibility, robustness, and environmental stability [1,2]. Few-layer graphene (FLG) with less than ten layers each shows a distinctive band structure [3]. This makes one interested in the physics of FLGs and their applications in useful devices [4,5]. There are different stacking ways for FLGs, such as AB and AA for bilayer (BLG or 2LG), trilayer (3LG), four-layer graphene (4LG), ABC for 3LG, and other stacking configurations [6]. The stacking configuration dominates the band structures of graphene layers. One stacking configuration, frequently discussed recently, is twisted bilayer graphene [$t(1 + 1)$ LG] [7]. $t(1 + 1)$ LG can be grown epitaxially on SiC(000 $\bar{1}$) surface [8,9] or by chemical vapor deposition (CVD) on Cu/Ni or other substrates [10,11]. In $t(1 + 1)$ LG, two Dirac linear electronic bands are coupled by a periodic interaction, with a large supercell, which can restore a Dirac-like linear dispersion with lower Fermi velocity than SLG [7,12,13]. $t(1 + 1)$ LG has two Van Hove singularities in its electronic density of states [14]. They can be resonant with incident laser with corresponding energy during the Raman scattering process and make the G peak extremely enhanced in intensity [15,16]. The G -band Raman intensity is calculated for twisted bilayer graphene as a function of laser excitation energy based on the extended tight-binding method [17]. R and R' bands are found to be from the scattering of TO and LO phonon in the center of the Brillouin zone by superlattice vector [18]. Carozo *et al.* studied the resonance effects in the Raman spectra (R , G , and $2D$ band) of $t(1 + 1)$ LG [19].

A graphene sheet can be rolled up to form graphene scroll [20–25]. Such graphene scroll shows unique properties and has potential applications in hydrogen storage, energy storage, and microcircuit interconnect [21,22,24]. This structure can be formed at the edges of SLG sample prepared by a micromechanical exfoliation method [20,22,25]. In the micromechanical exfoliation process to produce graphene layers, similar scroll structures can also be formed at edges of few layer graphenes. For example, 2-4LGs can be rolled up at edges to form 2-4 layer graphene scrolls (2-4LGSs).

Raman spectroscopy is used to probe graphene samples, as one of the most useful and versatile tools [26,27]. The measurement of Raman spectra of SLG, BLG, and FLG is a good way to understand their physical properties, such as phonons, electron-phonon, magnetophonon, and electron-electron interactions [27,28]. In bulk graphite, besides the G modes at 1582 cm^{-1} , there are another two degenerate E_{2g} modes at 42 cm^{-1} [29–31]. As a result of the weak interlayer coupling in graphite, the G -mode frequency exhibits no obvious difference in intrinsic (undoped) SLG, BLG, FLG, and bulk graphite [27]. The E_{2g} mode at 42 cm^{-1} in graphite corresponds to in-plane shear displacements between adjacent layers [31,32]. Because this shear mode provides a direct measurement of the interlayer coupling, it is named as the C mode [31]. As adjacent layers are rigidly displaced with respect to each other against the weak interlayer restoring force, the C mode is not usually observed in typical Raman spectra for graphite samples due to its weak intensity and low frequency [31,33]. Recently, using three BraggGrate notch filters (BNF) in combination with a single monochromator with high throughput, the C modes of BLG and FLGs were measured [31]. The experimental results agreed very well with a linear-chain model [31]. Similar C modes were then found in other two-dimensional materials, such as MoS₂ [34] and WSe₂ [35]. Based on the symmetric analysis, for FLG with N layers,

^{*}phtan@semi.ac.cn

there are $N - 1$ pairs of degenerate in-plane C modes [31]. Up to now, only the C mode with the highest frequency has been observed in FLGs. Because other Raman-active C modes have a much weaker intensity than the one with the highest frequency as a result of a much smaller electron-phonon coupling [31], it is a challenge to detect these low-frequency C modes.

In this paper, in contrast to the fact that only one C mode with the highest frequency is observed in 2-4LGs, we have observed all the C modes of 2-4LGs in the Raman spectra of 2-4LGSs at the edges of 2-4LGs. The C mode of 2-4LGs were measured for comparison. The observed frequencies of all the C modes agree well with the theoretical prediction for 3-4LGs. The results show clear evidence that the layer coupling in FLGs will strongly modify the corresponding phonon spectra in the lower frequency region, which has not been experimentally demonstrated clearly until now for such a layered system.

II. EXPERIMENT

In this work, graphene samples were obtained by micromechanical cleavage of natural graphite on the surface of a Si wafer chip with 293 or 92 nm thick SiO_2 on the top [36]. 2-4LGs with a Bernal stacking were identified by Raman spectra from their spectral profiles of the $2D$ mode [37]. Raman measurements were performed in a backscattering geometry at room temperature using a Jobin-Yvon HR800 Raman system. The excitation wavelengths are 633 nm of a He-Ne laser and 532 nm of a diode pumped solid-state laser. The laser excitations were cleaned from their plasma lines with BraggGrate bandpass filters. Measurements of Raman modes with frequencies close to 5 cm^{-1} were enabled by three BraggGrate notch filters at 633 or 532 nm with optical density 3 and with the full width at half maximum (FWHM) of $5\text{--}10 \text{ cm}^{-1}$. Both BraggGrate bandpass and notch filters are produced by OptiGrate Corp. All the Raman measurements were done using a $100\times$ objective lens ($\text{NA} = 0.90$) and a 1800 lines/mm grating to get a spectral resolution 0.35 cm^{-1} per CCD pixel. By monitoring the G peak position [38], we found that a laser power of 0.5 mW is safe to avoid sample heating.

III. RESULTS AND DISCUSSION

We first discuss the first- and second-order Raman modes of bulk graphite, as shown in Fig. 1. All the Raman modes in Fig. 1 are with the same scales of intensity and wave number. The asymmetrical peak at about 2700 cm^{-1} is the second order of the D peak, which is due to the breathing modes of six-atom rings [27]. The peak at about 3250 cm^{-1} is the second order of the D' peak, which is at about 1620 cm^{-1} in defected graphite measured at 514 nm. The D and D' bands require a defect for their activation by intervalley and intravalley double resonance Raman processes [39–41], respectively. Therefore, they are absent in pure graphite. In the lower frequency region, a pair of Stokes and anti-Stokes modes are found at 43.5 cm^{-1} , which is close to the value of 42 cm^{-1} for the C mode in a few previous reports [29,30]. Here the simultaneous measurement of Stokes and anti-Stokes signal enables a precise determination of the frequency of the shear mode [31]. The FWHM of the G peak

in graphite is as large as 12.0 cm^{-1} , which is dominated by its electron-phonon coupling strength because of its nature of semimetal [42]. However, The FWHM of the C mode is very narrow, only 1.6 cm^{-1} . If we exclude the instrument broadening of 0.6 cm^{-1} , which can be estimated from the broadening of laser excitation in the Raman spectra, the intrinsic FWHM of the C mode is as narrow as 1.0 cm^{-1} . As shown in Fig. 1, the peak intensity of the C mode $I(C)$ is about 7% of $I(G)$, while the area intensity $A(C)$ is about 0.6% of $A(G)$ due to the narrow width of the C mode. The weak intensity, narrow width, and low frequency of the C mode make it difficult to be observed in the single stage spectrograph with a normal notch (or edge) filter and also in the triple monochromator system [31].

The high frequency modes ($\geq 200 \text{ cm}^{-1}$) of graphite and graphene layers have been widely investigated up to now [27]. However, only a few works reported on the low frequency Raman modes of these materials [29–31]. Here we focus on the ultralow-frequency modes of few layer graphene scrolls. Figure 2 shows the schematic diagram of 2LGS in a cross-sectional view and a side view, optical images of 2-3LGS and the corresponding 2-3LGSs at their edges, and their Raman spectra. Under the excitation of 633 nm, the layer number of suspended/supported 2-4LGs can be easily identified from the line shape of the $2D$ peak [37]. Indeed, the suspended 2LG and supported 3LG located at position 2A and 3A in Figs. 2(b) and 2(c), respectively, exhibit typical $2D$ peaks of 2LG and 3LG, as shown in Figs. 2(d) and 2(e). In the low frequency region, one Raman mode was observed for each 2LG and 3LG, respectively, at 31 and 38 cm^{-1} . These modes could be assigned to the C mode in analogy to that in graphite according to their frequency regions [31]. Their frequency is lower than that (43.5 cm^{-1}) in graphite. Although its intensity is very weak, it can be identified from the strong background as indicated by arrows in Fig. 2. There are 2LGS and 3LGS structures, respectively, located at the edges of the 2LG and 3LG in Figs. 2(b) and 2(c). The Raman spectra of 2-3LGSs at positions 2B and 3B, respectively, show similar $2D$ profiles of the 2-3LGs with a blueshift of several wave number in frequency, which is an analogy to the case in $t(1 + 1)$ LG. This was attributed to the reduction of Fermi velocity at Dirac point

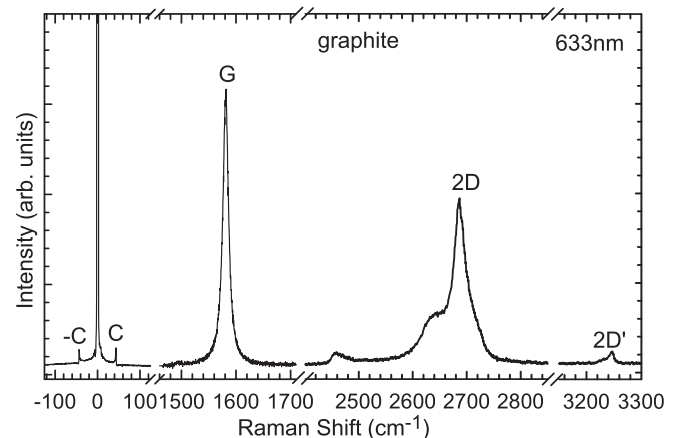


FIG. 1. First- and second-order Raman spectra of bulk graphite excited by 633 nm excitation.

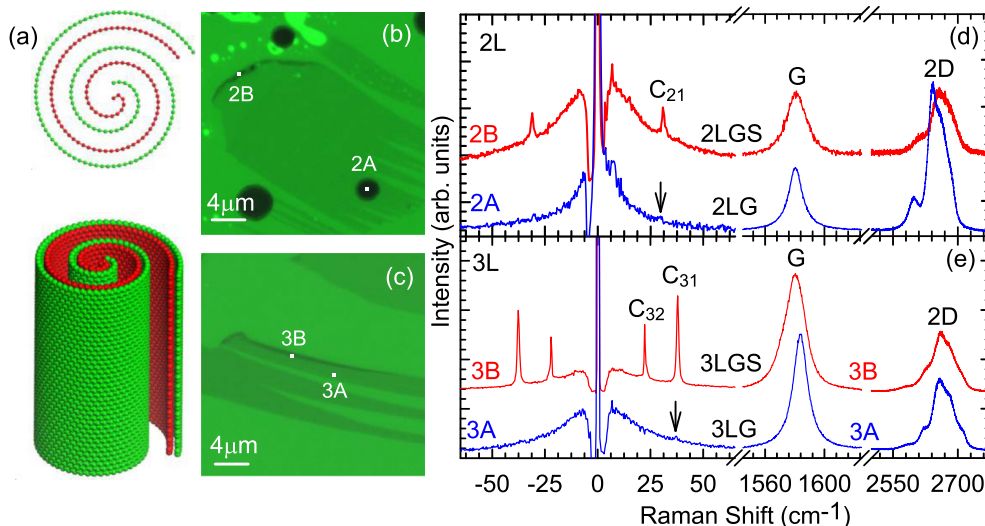


FIG. 2. (Color online) (a) Schematic diagram of 2LS in a cross-sectional view (top) and a side view (bottom). (b) Optical images of 2LA (2A) and 2LGS at edges (2B). (c) Optical images of 3LA (3A) and 3LGSs at edges (3B). (d) and (e) Raman spectra of 2-3LGs [(2A) and (3A)] and 2-3LGSs [(2B) and (3B)] in the low frequency region, G- and 2D-band regions.

[12,16]. The G mode of 2-3LGSs still exhibits a Lorentzian line shape while its width is slightly broadened in comparison to that of 2-3LGs. However, the C mode in 2-3LGs is strongly enhanced in the 2-3LGSs. In principle, because 2-3LGSs are formed from 2-3LGs, more graphene layers in scrolls can significantly increase the intensity of the corresponding C mode. We will discuss it in detail later. Interestingly, an additional mode was observed at 22 cm⁻¹ in the 3LGS.

Figure 3 shows the optical image and Raman spectra of a 4LG and the corresponding 4LGS and the twisted 8LG [*t*(4 + 4)LG] folded by 4LGs. The Raman spectra at position 4A excited by 633 nm shows a typical spectral feature of 4LG [37] and its C mode was observed at 40 cm⁻¹. The multiple structures of the 2D peak of 4LG was smeared out in the

t(4 + 4)LG at position 4B, while the intensity of the C mode at 40 cm⁻¹ is twice as much as that in 4LG at 4A. Similar to 3LGS, 2D mode in 4LGS at position 4C moves to higher frequency in comparison to that in 4LG at 4A. However, in the low frequency region, two additional modes were observed at 17 and 31 cm⁻¹ in 4LGS. To further confirm these Raman features, a 532 nm laser was utilized for the 4LGS at 4C. Again, three modes were observed with identical frequencies to those excited by the 633 nm excitation, respectively.

To reveal the nature of additional modes observed in the low frequency region of 3-4LGSs, the phonon modes of FLGs were calculated based on a force constant model [43] and a linear chain model [31]. According to the symmetrical analysis of an *n* (*n* ≥ 2) layer graphene (*n*LG) [43,44], there are *n* pairs of degenerate in-plane stretching modes and *n* - 1 pairs of degenerate in-plane C modes between neighboring layers. The former corresponds to the feature in the G-band region and the latter appears in the low frequency region. If one uses *C_{nm}* to denote the *m*th C mode (*m* = 1, 2, ..., *n* - 1) of *n*LGs and the mode with the highest frequency is *C_{n1}*, the C modes observed in *n*LGs is actually the *C_{n1}* mode [31]. In principle, there are one, two, and three pairs of degenerate C modes in 2LG, 3LG, and 4LG, respectively. The force-constant model [43] is adopted to calculate the frequency of the C mode and the G band in bulk graphite and 2-4LGs, in which 15 parameters are used to describe fifth-nearest neighbor force constants of intralayer and 8 parameters for fourth-nearest-neighbor force constants of interlayer. The theoretical values for the two Raman-active degenerate *E_{2g}* modes of graphite are, respectively, at 1581.7 and 42.0 cm⁻¹. The former is the in-plane stretching mode, i.e., the G mode. The latter is the in-plane C mode between adjacent graphene layers in graphite. The theoretical frequencies of bulk graphite are consistent with the experimental ones in Fig. 1. The theoretical frequencies of all the C modes are summarized in Table I along with the experimental results of 2-4LGs and 2-4LGSs. The *C_{n1}* mode frequencies (*n* = 2, 3, 4) observed in 2-4LGs, respectively,

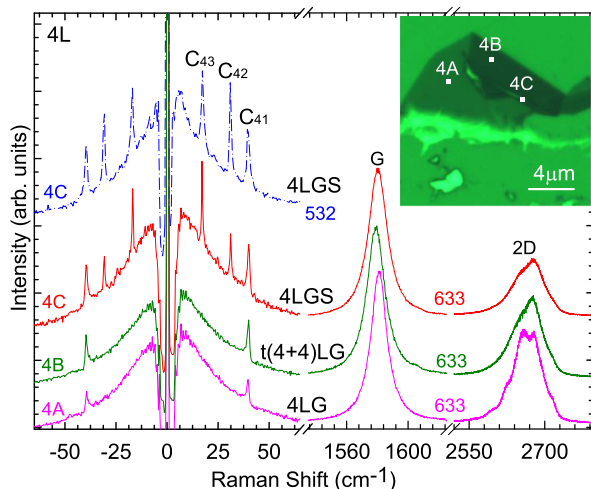


FIG. 3. (Color online) Raman spectra of 4LG (4A), *t*(4 + 4)LG (4B), and 4LGS (4C) in the low frequency region by 633 and 532 nm excitations and G- and 2D-band regions by 633 nm excitation. The inset gives the optical image of 4LG, the corresponding 4LGS and *t*(4 + 4)LG.

TABLE I. Theoretical (Theor.) values (in cm^{-1}) of the C modes in 2-4LGs based on the force constant model (FCM) and linear chain model (LCM), and the corresponding experimental (Expt.) ones in 2-4LGs and the corresponding scrolls (2-4LGSs). The notation of each observed C mode of 2-4LGSs in Figs. 2 and 3 are indicated within parentheses after the experimental values.

Mode	2L		3L		4L	
	$E_g(R)$	$E''(R,IR)$	$E'(R)$	$E_g^2(R)$	$E_u(IR)$	$E_g^1(R)$
Theor. (FCM)	32.0	37.8	23.4	39.7	32.0	18.2
Theor. (LCM)	30.8	37.7	21.8	40.2	30.8	16.7
Expt. in 2-4LGs	30.0	37.2	–	39.2	–	–
Expt. in 2-4LGSs	31.2 (C_{21})	37.6 (C_{31})	21.9 (C_{32})	39.5 (C_{41})	30.7 (C_{42})	16.7 (C_{43})

agree with the theoretical ones by the force-constant model. Both theoretical and experimental results show that the C_{n1} mode significantly reduces in frequency with decreasing the layer number. The theoretical values of the other C modes, i.e., E' mode in 3LGs, and E_u and E_g^1 modes in 4LGs, agree with those of additional modes observed in 3-4LGSs in Figs. 2(e) and 3. This suggests that all the C modes of 3-4LGs were observed in 3-4LGSs at edges of 3-4LGs. For example, the modes at 37.6 and 21.9 cm^{-1} in the 3LGS, respectively, correspond to the C_{31} and C_{32} mode in the 3LG. All the observed shear modes in 2-4LGSs are labeled with corresponding denotations in Figs. 2(d), 2(e), and 3. The observed C_{32} and C_{43} modes of 3-4LGSs are, respectively, attributed to the C mode of two outer layers with respect to center layer(s) of 3-4LGs, and the C_{42} mode of 4LGS is attributed to the C mode between top and bottom two layers of the 4LG [31]. Table I also includes the theoretical results of the C mode frequencies based on the linear chain model [31], which also agrees with the experimental results.

In principle, the C modes are collective vibrations of all the graphene layers in 2-4LGSs. However, the number and the frequency of the observed C modes in 2-4LGSs are almost the same as those in 2-4LGs. This suggests that the coupling between adjacent layers n LGSs is slightly different from that of Bernal-stacked n LG. Because there are local strain, layer stacking slightly beyond from the Bernal-stacked case

for n LGs in n LGSs and slightly different coupling between adjacent layers in n LGSs, it is reasonable that the frequency of the experimentally observed C modes in n LGSs is slightly different from that calculated from the linear chain model, as shown in Table I.

The C_{42} mode observed in 4LGSs in Fig. 3 (i.e., the E_u mode of the 4LG in Fig. 3(b) of Ref. [31]) is infrared active and Raman inactive. Indeed, it is absent in supported 4LGs. The C_{32} and C_{43} modes of 3-4LGSs in Figs. 2(e) and 3 are Raman active, however, they are also absent in supported 3-4LGs. The absence of the C_{32} and C_{43} modes in 3-4LGs results from their weak Raman cross section [31]. However, these modes can be stronger than the C_{31} and C_{41} modes in 3-4LGSs as indicated in Figs. 2(e) and 3. The modification of crystalline point-group symmetry in graphene scrolls can relax wave-vector selection rule by loss of translational symmetry and make infrared C_{42} mode Raman active, similar to the observation of Raman-inactive B_{2g} mode at 867 cm^{-1} at the edge plane of graphite [45]. However, its strong intensity in the 4LGSs is still an unexpected result. Furthermore, the C mode intensity in the 3LGSs in Fig. 3 is independent on the the optical contrast of graphene flakes, i.e., the number of graphene layers of the 3LGSs. All the aspects point to that all the C modes in 2-4LGSs are resonantly enhanced in some local positions so that the Raman-inactive or absent Raman modes in supported 3-4LGs become visible in 3-4LGSs.

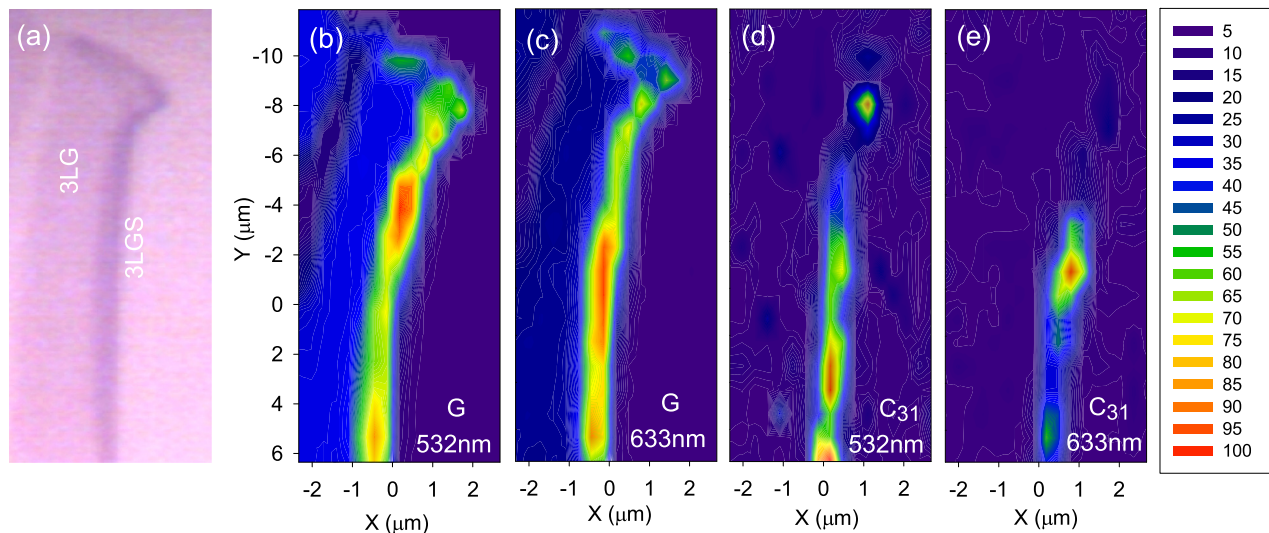


FIG. 4. (Color online) (a) Optical image of the 3LG and 3LGSs. The pseudocolor Raman images of the area intensity of the G mode by 532 nm (b) and 633 nm (c) excitations, and those of the C_{31} mode by 532 nm (d) and 633 nm (e) excitations.

To reveal the physical origin of the possible intensity resonance of the C mode, we performed Raman mapping of the C and G modes upon the 3LGSs by 532 and 633 nm laser excitations, where the optical image is plotted in Fig. 4(a) for reference. The results are depicted in Figs. 4(b)–4(e). The area intensities of both the G mode, $A(G)$, and the C_{31} mode, $A(C)$, are independent on the optical contrast of the 3LGSs. Especially, Raman images of both the G and C_{31} modes by the 532 nm excitation are quite different from those by the 633 nm excitation, respectively. This provides direct evidence that both the C and G modes are resonantly enhanced in intensity at some spots by a specific excitation. The resonant region of the C mode of 3LGSs in Figs. 4(d) and 4(e) is much narrower than that of the G band.

The intensity enhancement of all the C modes in 2-4LGSs reveals that their electronic structures are quite different from those of the corresponding 2-4LGs. It is impossible to calculate the electronic structures of real few layer graphene scrolls because of its complex stacking configuration, different local twisted angle, and possible curvatures. For a very simple assumption, here we consider how the band structures of twisted $(n+n)$ layer graphenes [$t(n+n)$ LGs, n is the layer number of Bernal-stacked few-layer graphenes, $n = 2, 3, 4$] change with the layer number and the twisted angle. The twisted angle of the $t(n+n)$ LG is determined by the rolling orientation [18]. Similar to $t(1+1)$ LG, the folding of one n LG on another n LG would form a hexagonal superlattice, as shown in Fig. 5(a) for the $t(2+2)$ LG as an example.

The reduced Brillouin zone of the $t(2+2)$ LG in Fig. 5(a) is plotted in Fig. 5(b). In $t(1+1)$ LG, there are two Van Hove singularities in the joint density of states (JDOS) [14],

which result from the parallel conduction and valence bands of its band structure [15,17]. During the Raman process, specific excitation with an energy close to the gap of these parallel bands will increase the transition probability and increase the G mode intensity [15–17]. We utilize DFTB+ program [46] to calculate the band structure of $t(n+n)$ LGs ($n = 2, 3, 4$). DFTB+ is an approximate density functional theory method based on the tight-binding approach that utilizes an optimized minimal linear combination of atomic orbital (LCAO) Slater-type all-valence basis set and a two-center approximation for Hamiltonian matrix elements. As shown in Fig. 5(c), the almost parallel bands still exist in $t(n+n)$ LG along the G-K (transition energy, E_{22}), G-M (E_{11}) and K-M (E'_{11}) directions. These parallel bands can form the Van Hove singularities in the JDOS, which can contribute to the intensity enhancement of Raman modes. For the same twisted angle in $t(n+n)$ LG ($n = 2, 3, 4$), for example 9.4° , their transition energies in the JDOS are almost the same to each other, and $E_{11} \approx E'_{11} \sim 1.8$ eV. However, if the twisted angle changes to 13.2° , the transition energies of E_{11} , E'_{11} and E_{22} are significantly changed, and $E_{11} \approx E'_{11} \sim 2.4$ eV for $t(4+4)$ LG in Fig. 5(c4). For a well-stacked $t(1+1)$ LG, the intensity resonance of the G mode by the transition gap has been observed [15,16], and specific laser excitations can be used to probe $t(1+1)$ LG with different twisted angles.

In the scroll structures formed from n LGs, the irregular rolling in the local areas will result in different local twisted angle and local strain due to curvatures at different measured spots. Once the excitation energy is resonant with the transition gaps between their conduction and valence bands of local scroll structures with proper twisted angles and strains, the C

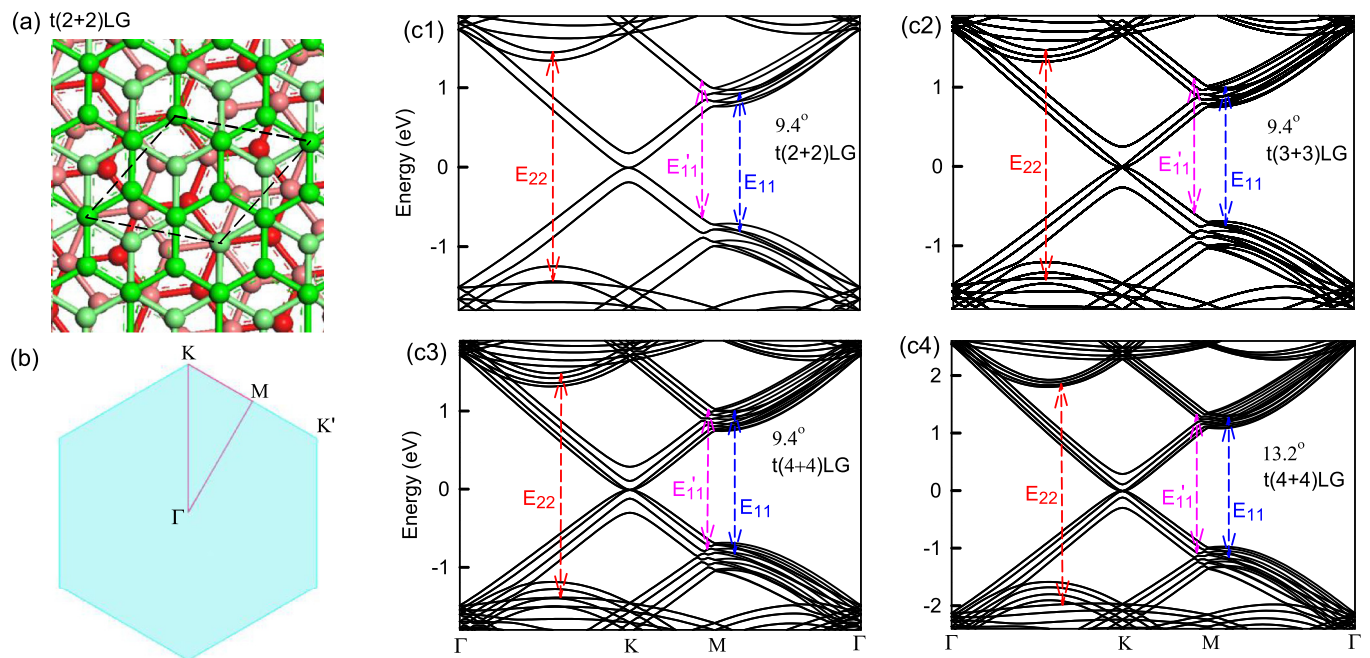


FIG. 5. (Color online) (a) Superlattice of a $t(2+2)$ LG with a twisted angle of 21.8° , here the green and light green layers and the red and light red layers are Bernal-stacked graphene bilayers. (b) Corresponding (reduced) Brillouin zone of the superlattice and its high-symmetry points. (c) Electronic band structure of $t(n+n)$ LGs ($n = 2, 3, 4$). (c1), (c2), and (c3), respectively, correspond to that of $t(2+2)$ LGs, $t(3+3)$ LGs, and $t(4+4)$ LGs with a twisted angle of 9.4° . (c4) $t(4+4)$ LGs with a twisted angle of 13.2° . All the band structures show several pairs of parallel conduction and valence bands with gaps of E_{11} , E'_{11} , and E_{22} , respectively, along Γ -M, K-M, and Γ -K directions.

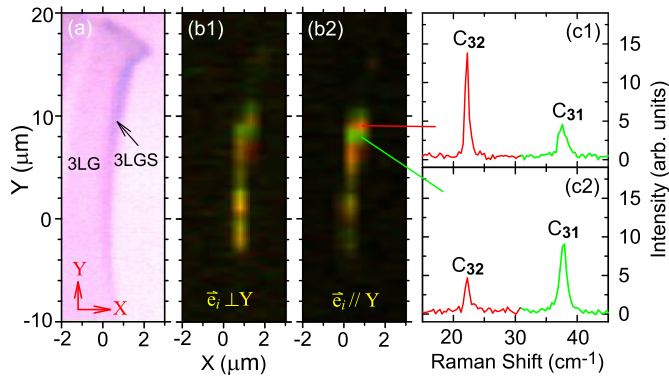


FIG. 6. (Color online) Optical image (a) of the 3LG and 3LGSs and the corresponding pseudocolor Raman image (b1) and (b2) by 633 nm when the laser polarization \vec{e}_i is, respectively, parallel and perpendicular to the Y axis, where the red and green colors reflect the Raman intensity of the C_{32} (22 cm^{-1}) and C_{31} (38 cm^{-1}) modes, respectively. Two typical Raman spectra in the image of (b2) are shown in (c1) and (c2).

mode intensity will be resonantly enhanced even the C mode is Raman inactive. In this case, the resonance condition of the C modes can be dependent on the excitation energy and the measured spots, as shown in Figs. 4(d) and 4(e). It is the similar case for the resonance of the G mode in n LGSs. It must be noted that the phonon energy of the C mode ($\sim 5\text{ meV}$) is very small, and thus its incoming resonance with excitation photons and outgoing resonance with scattered photons can be simultaneously satisfied. This will result in a small resonance window in energy for a specific twisted angle. However, the phonon energy of the G mode is as large as $\sim 0.2\text{ eV}$, which means that its resonance window in energy is much broader than that of the C mode. This explains why the resonant spot size of the C mode in Figs. 4(d) and 4(e) is smaller than that of the G mode in Figs. 4(b) and 4(c).

Most graphene scrolls have a wire morphology in the local area at the sample edge. Raman spectra with parallel (YY) and perpendicular (XY) polarization configuration for incident and scattered light are collected upon the 3LGSs in Fig. 2(c). The optical image and polarization configuration are shown in Fig. 6(a). We have recorded the backscattering Raman signal with polarization along the Y direction. A half-wave plate is used to change the polarization direction of the incident excitation \vec{e}_i along either parallel (Y) or perpendicular (X) to the Raman signal. Raman images with (XY) and (YY) configurations are shown in Figs. 6(b1) and 6(b2). The peak intensity of the C_{31} and C_{32} modes is, respectively, displayed in the images in green and red colors. Therefore, both the intensity and intensity ratio of the C_{31} and C_{32} modes are

demonstrated in images as the brightness with different colors. For instance, Figs. 6(c1) and 6(c2) show Raman spectra at different spots in Fig. 6(b2). The images show that the peak intensity and polarization of the C_{31} and C_{32} modes, and intensity ratio between the C_{31} and C_{32} modes are dependent on the measured position. The C mode is too weak to be observed for the supported 3LG and for the top and bottom parts of 3LGSs. Therefore, the strong C_{31} and C_{32} modes in graphene scrolls could not be related to more graphene layers in 3LGSs, but to the resonance by local band structures of graphene scrolls as discussed above.

The D , G , and $2D$ bands may show polarization dependence of modes intensity in graphene and at graphene edge [47–51]. In principle, n LGSs usually show wire morphology in the local area at the sample edge. This may result in anisotropy of the light absorption in n LGSs and lead to the polarization of the C modes in analog to the G mode in nanographite ribbons [51]. However, as shown in Figs. 6(b1) and 6(b2), the polarization dependence of the C_{31} and C_{32} modes is not uniform along the 3LGS axis. We prefer to attribute this to the different resonant behaviors of the C_{31} and C_{32} modes along the 3LGS axis, which results from the significantly different band structures due to the complex local stacking configuration.

IV. CONCLUSIONS

In conclusion, the one, two, and three low frequency modes below 50.0 cm^{-1} are observed in the Raman spectra of 2-4LGSs, which are attributed to the Raman- and infrared-active in-plane C mode between neighbor layers of 2-4LGs according to the theoretical results based on the force-constant and linear chain models. All the C modes are with a narrow linewidth less than about 1.4 cm^{-1} . In addition, the C mode intensity and polarization are dependent on the measured spot, attributed to the intensity enhancement by the electronic transition gaps of band structures in graphene scrolls, which are strongly dependent on the spatially different local stacking configuration. This observation of all the C modes in 3-4LGSs reveals the interlayer coupling in few layer graphenes in detail and comprehensively, which can be extended to other two-dimensional materials with similar scroll structures.

Note added. Recently, we became aware of a reprint reporting similar results on folded graphene Layers [52].

ACKNOWLEDGMENTS

This work was supported by the National Basic Research Program of China (973 Program) Grant No. 2009CB929301, and National Natural Science Foundation of China under Grant No. 10934007 and No. 11225421.

- [1] A. K. Geim and K. S. Novoselov, *Nat. Mater.* **6**, 183 (2007).
- [2] F. Bonaccorso, Z. Sun, T. Hasan, and A. Ferrari, *Nat. Photon.* **4**, 611 (2010).
- [3] M. Koshino and T. Ando, *Solid State Commun.* **149**, 1123 (2009).

- [4] W. Zhu, V. Perebeinos, M. Freitag, and P. Avouris, *Phys. Rev. B* **80**, 235402 (2009).
- [5] J. Ye, M. F. Craciun, M. Koshino, S. Russo, S. Inoue, H. Yuan, H. Shimotani, A. F. Morpurgo, and Y. Iwasa, *Proc. Natl. Acad. Sci. USA* **108**, 13002 (2011).

- [6] C. H. Lui, Z. Li, Z. Chen, P. V. Klimov, L. E. Brus, and T. F. Heinz, *Nano Lett.* **11**, 164 (2010).
- [7] J. M. B. Lopes dos Santos, N. M. R. Peres, and A. H. Castro Neto, *Phys. Rev. Lett.* **99**, 256802 (2007).
- [8] C. Berger, Z. Song, X. Li, X. Wu, N. Brown, C. Naud, D. Mayou, T. Li, J. Hass, A. N. Marchenkov, E. H. Conrad, P. N. First, and W. A. de Heer, *Science* **312**, 1191 (2006).
- [9] J. Hass, F. Varchon, J.-E. Millan-Otoya, M. Sprinkle, N. Sharma, W. A. de Heer, C. Berger, P. N. First, L. Magaud, and E. H. Conrad, *Phys. Rev. Lett.* **100**, 125504 (2008).
- [10] K. S. Kim, Y. Zhao, H. Jang, S. Y. Lee, J. M. Kim, K. S. Kim, J.-H. Ahn, P. Kim, J.-Y. Choi, and B. H. Hong, *Nature (London)* **457**, 706 (2009).
- [11] A. Reina, X. Jia, J. Ho, D. Nezich, H. Son, V. Bulovic, M. S. Dresselhaus, and J. Kong, *Nano Lett.* **9**, 30 (2009).
- [12] Z. Ni, Y. Wang, T. Yu, Y. You, and Z. Shen, *Phys. Rev. B* **77**, 235403 (2008).
- [13] G. Trambly de Laissardière, D. Mayou, and L. Magaud, *Nano Lett.* **10**, 804 (2010).
- [14] G. Li, A. Luican, J. L. Dos Santos, A. C. Neto, A. Reina, J. Kong, and E. Andrei, *Nat. Phys.* **6**, 109 (2009).
- [15] R. W. Havener, H. Zhuang, L. Brown, R. G. Hennig, and J. Park, *Nano Lett.* **12**, 3162 (2012).
- [16] K. Kim, S. Coh, L. Z. Tan, W. Regan, J. M. Yuk, E. Chatterjee, M. F. Crommie, M. L. Cohen, S. G. Louie, and A. Zettl, *Phys. Rev. Lett.* **108**, 246103 (2012).
- [17] K. Sato, R. Saito, C. Cong, T. Yu, and M. S. Dresselhaus, *Phys. Rev. B* **86**, 125414 (2012).
- [18] V. Carozo, C. M. Almeida, E. H. Ferreira, L. G. Cançado, C. A. Achete, and A. Jorio, *Nano Lett.* **11**, 4527 (2011).
- [19] V. Carozo, C. Almeida, B. Fragneaud, P. Bede, M. Moutinho, J. Ribeiro-Soares, N. Andrade, A. Souza Filho, M. Matos, B. Wang *et al.*, *Phys. Rev. B* **88**, 085401 (2013).
- [20] J. C. Meyer, A. Geim, M. Katsnelson, K. Novoselov, T. Booth, and S. Roth, *Nature (London)* **446**, 60 (2007).
- [21] Y. Chen, J. Lu, and Z. Gao, *J. Phys. Chem. C* **111**, 1625 (2007).
- [22] X. Xie, L. Ju, X. Feng, Y. Sun, R. Zhou, K. Liu, S. Fan, Q. Li, and K. Jiang, *Nano Lett.* **9**, 2565 (2009).
- [23] M. M. Fogler, A. H. Castro Neto, and F. Guinea, *Phys. Rev. B* **81**, 161408 (2010).
- [24] A. K. Schaper, M. S. Wang, Z. Xu, Y. Bando, and D. Golberg, *Nano Lett.* **11**, 3295 (2011).
- [25] R. Podila, R. Rao, R. Tsuchikawa, M. Ishigami, and A. M. Rao, *ACS Nano* **6**, 5784 (2012).
- [26] A. Ferrari, J. Meyer, V. Scardaci, C. Casiraghi, M. Lazzeri, F. Mauri, S. Piscanec, D. Jiang, K. Novoselov, S. Roth *et al.*, *Phys. Rev. Lett.* **97**, 187401 (2006).
- [27] A. C. Ferrari and D. M. Basko, *Nat. Nanotechnol.* **8**, 235 (2013).
- [28] A. C. Ferrari, *Solid State Commun.* **143**, 47 (2007).
- [29] R. Nemanich, G. Lucovsky, and S. Solin, *Solid State Commun.* **23**, 117 (1977).
- [30] K. Mani and R. Ramani, *Phys. Status Solidi B* **61**, 659 (1974).
- [31] P. Tan, W. Han, W. Zhao, Z. Wu, K. Chang, H. Wang, Y. Wang, N. Bonini, N. Marzari, N. Pugno *et al.*, *Nat. Mater.* **11**, 294 (2012).
- [32] R. J. Nemanich, G. Lucovsky, and S. A. Solin, in *Proceedings of the International Conference on Lattice Dynamics* (Flammarion, Paris, 1975), pp. 619–622.
- [33] M. Hanfland, H. Beister, and K. Syassen, *Phys. Rev. B* **39**, 12598 (1989).
- [34] X. Zhang, W. P. Han, J. B. Wu, S. Milana, Y. Lu, Q. Q. Li, A. C. Ferrari, and P. H. Tan, *Phys. Rev. B* **87**, 115413 (2013).
- [35] Y. Zhao, X. Luo, H. Li, J. Zhang, P. T. Araujo, C. K. Gan, J. Wu, H. Zhang, S. Y. Quek, M. S. Dresselhaus *et al.*, *Nano Lett.* **13**, 1007 (2013).
- [36] K. Novoselov, D. Jiang, F. Schedin, T. Booth, V. Khotkevich, S. Morozov, and A. Geim, *Proc. Natl. Acad. Sci. USA* **102**, 10451 (2005).
- [37] W. J. Zhao, P. H. Tan, J. Zhang, and J. Liu, *Phys. Rev. B* **82**, 245423 (2010).
- [38] P. Tan, Y. Deng, Q. Zhao, and W. Cheng, *Appl. Phys. Lett.* **74**, 1818 (1999).
- [39] C. Thomsen and S. Reich, *Phys. Rev. Lett.* **85**, 5214 (2000).
- [40] R. Saito, A. Jorio, A. G. Souza Filho, G. Dresselhaus, M. S. Dresselhaus, and M. A. Pimenta, *Phys. Rev. Lett.* **88**, 027401 (2001).
- [41] P. H. Tan, L. An, L. Q. Liu, Z. X. Guo, R. Czerw, D. L. Carroll, P. M. Ajayan, N. Zhang, and H. L. Guo, *Phys. Rev. B* **66**, 245410 (2002).
- [42] M. Lazzeri, S. Piscanec, F. Mauri, A. C. Ferrari, and J. Robertson, *Phys. Rev. B* **73**, 155426 (2006).
- [43] H. Wang, Y. Wang, X. Cao, M. Feng, and G. Lan, *J. Raman Spectrosc.* **40**, 1791 (2009).
- [44] L. M. Malard, M. H. D. Guimarães, D. L. Mafra, M. S. C. Mazzoni, and A. Jorio, *Phys. Rev. B* **79**, 125426 (2009).
- [45] Y. Kawashima and G. Katagiri, *Phys. Rev. B* **59**, 62 (1999).
- [46] B. Aradi, B. Hourahine, and T. Frauenheim, *J. Phys. Chem. A* **111**, 5678 (2007).
- [47] D. Yoon, H. Moon, Y.-W. Son, G. Samsonidze, B. H. Park, J. B. Kim, Y. Lee, and H. Cheong, *Nano Lett.* **8**, 4270 (2008).
- [48] R. Yang, Z. Shi, L. Zhang, D. Shi, and G. Zhang, *Nano Lett.* **11**, 4083 (2011).
- [49] E. B. Barros, K. Sato, G. G. Samsonidze, A. G. Souza Filho, M. S. Dresselhaus, and R. Saito, *Phys. Rev. B* **83**, 245435 (2011).
- [50] C. Casiraghi, A. Hartschuh, H. Qian, S. Piscanec, C. Georgi, A. Fasoli, K. Novoselov, D. Basko, and A. Ferrari, *Nano Lett.* **9**, 1433 (2009).
- [51] L. G. Cançado, M. A. Pimenta, B. R. A. Neves, G. Medeiros-Ribeiro, T. Enoki, Y. Kobayashi, K. Takai, K.-i. Fukui, M. S. Dresselhaus, R. Saito, and A. Jorio, *Phys. Rev. Lett.* **93**, 047403 (2004).
- [52] C. Cong and T. Yu, [arXiv:1312.6928](https://arxiv.org/abs/1312.6928).